Scientific Research Publishing

Advances in Materials Physics and Chemistry, 2026, 16(3), 121-143
https://www.scirp.org/journal/ampc
ISSN Online: 2162-5328
ISSN Print: 2162-531X

Camel Manure-Derived Biochar/Fe_3O_4 Nanocomposite as a Sustainable Adsorbent for Pb(II) and Cd(II) Removal from Wastewater

Nabil Abduraqeb Alhemiary[1,2*], Mohammed Ali Helmi[3]

[1]Department of Chemistry, Faculty of Science and Arts, Najran University, Najran, Saudi Arabia
[2]Department of Chemistry, Faculty of Science, Ibb University, Ibb, Yemen
[3]Departement of Analytical Chemistry, Faculty of Pharmacy, Helwan University, Cairo, Egypt
Email: nafarhan@nu.edu.sa

How to cite this paper: Alhemiary, N.A. and Helmi, M.A. (2026) Camel Manure-Derived Biochar/Fe_3O_4 Nanocomposite as a Sustainable Adsorbent for Pb(II) and Cd(II) Removal from Wastewater. *Advances in Materials Physics and Chemistry*, **16**, 121-143.
https://doi.org/10.4236/ampc.2026.163006

Received: January 11, 2026
Accepted: March 1, 2026
Published: March 4, 2026

Abstract

This study synthesizes a magnetic biochar nanocomposite from camel manure via pyrolysis and co-precipitation to remove lead and cadmium from aqueous solutions. The researchers characterize the material using FTIR, XRD, SEM-EDX, and XPS, confirming the presence of iron oxide and surface functional groups. Batch adsorption experiments indicate that the composite achieves high removal efficiencies (97.46% for Pb and 99.17% for Cd) following pseudo-second-order kinetics.

Keywords

Camel Manure-Derived, Biochar, Wastewater, Removal of Heavy Metal, Iron Oxide

1. Introduction

Heavy metal contamination of aquatic systems represents one of the most persistent environmental challenges due to their non-biodegradable nature, toxicity, and tendency for bioaccumulation [1]. Anthropogenic activities such as industrial discharge, agricultural runoff, mining operations, and urban expansion significantly contribute to the continuous release of toxic metal ions into water bodies [2]. Once introduced into the environment, these metals persist for extended periods and may enter the food chain, posing serious risks to ecosystems and human health [3]. Numerous heavy metals in their ionic state are toxic or carcinogenic [4]. The levels of heavy metals in soil, groundwater, and different water bodies surpass acceptable limits in several nations due to unplanned urbanization, indus-

try, population increase, and inadequate management regulations, posing a latent threat to the human food chain [4]. Cd(II) is detrimental to both animals and humans, potentially resulting in several long-term and short-term health problems [5]. Cadmium(II) can enter the body by inhalation, ingestion, or dermal absorption. Brief exposure to cadmium can induce vomiting, diarrhea, spasms, peripheral neuropathy, hepatic damage, seizures, shock, alterations in renal function, and adverse effects on the lungs, circulatory system, liver, and neurological system [6]. Furthermore, cadmium can impact the lungs, kidneys, bones, and growth, and may induce cancer over time [7]. Finally, Pb(II) is a very toxic and accumulative toxin that predominantly deposits in the kidneys, bones, muscles, and brain [8]. Chronic lead poisoning adversely affects the kidneys, neurological and reproductive systems, brain, and liver [9]. Conventional wastewater treatment technologies, including membrane filtration, ion exchange, coagulation, electrochemical treatment, and reverse osmosis, have been employed to mitigate heavy metal contamination [10]. However, these methods often suffer from high operational costs, energy consumption, incomplete removal at high metal concentrations, and the generation of secondary pollutants. Consequently, the development of cost-effective, environmentally benign, and sustainable materials for heavy metal remediation has become a research priority [11]. As a result, there is a need for affordable and environmentally acceptable biomaterials to remove environmental pollutants. According to published research, biomaterials for the removal of environmental contaminants, such as algae [12], bacteria [13], fungi [14], plants [15], serve as environmentally benign and cost-effective biosorbents for the elimination of environmental contaminants.

Biochar, a carbon-rich material obtained through the thermal decomposition of biomass under oxygen-limited conditions, has emerged as a promising adsorbent owing to its porous structure, surface functional groups, chemical stability, and low production cost [16]-[18]. Biochars derived from animal manure are particularly attractive due to their high mineral content, surface heterogeneity, and contribution to waste valorization [19] [20]. Several studies have demonstrated the effectiveness of manure-based biochars in immobilizing metal ions through surface complexation, ion exchange, and precipitation mechanisms. The dairy dung-derived biochar removed Cu, Zn, and Cd from water. Mostly, biochar precipitates metal ions with PO_4^{3-} and CO_3^{2-} ions to adsorb metals [21]. Biochar produced from cow and pig manure adsorbs Cu(II) metal ions (>88 mg/g) and Pb(II) (>200 mg/g) [22].

The efficiency of biochar made from co-pyrolyzing swine dung and corn straw for adsorbing metal ions including Ni, Cu, and Pb was studied. Chicken manure biochar also adsorbs Pb(II) ions from aqueous solutions [23]. Batool *et al.* found that biochar made from farmyard and chicken manures removed Cu(II) best at pH 2 [24].

Additionally, it has been shown that modified yak dung has enhanced adsorption capacities for heavy metals such as Pb(II), Cu(II), Cd(II), and Zn(II) ions.

According to the study, Pb(II) absorption capacity increased from 76.41 mg/g to 169.57 mg/g when yak dung biochar was treated with H_2O_2 [25].

In Saudi Arabia, camel husbandry generates substantial quantities of organic waste, which remain underutilized despite their significant resource potential. There are two million camels in Saudi Arabia, as per the Ministry of Environment, Water, and Agriculture [26]. Daily dung production by mature drought camels averages 8 - 11 kg, with higher yields for dairy camels [27]. When accumulated annually, this amounts to about 4 million tons. However, this waste is now being used on a modest scale in Saudi Arabia, primarily as fertilizer for farmers. Transforming camel manure into functional biochar provides an environmentally sustainable solution for waste management while offering a low-cost material for wastewater treatment. Therefore, this study aims to synthesize camel manure-derived biochar modified with iron oxide nanoparticles and evaluate its efficiency for the removal of Pb(II) and Cd(II) ions from aqueous solutions. The adsorption performance is systematically investigated under varying experimental conditions, including pH, contact time, adsorbent dosage, and initial metal concentration, to assess its potential applicability in environmental remediation.

2. Material and Methods

2.1. Chemicals

The solution was prepared using iron chloride hexahydrate ($FeCl_3 \cdot 6H_2O$). Copper sulfate hexahydrate ($CuSO_4 \cdot 5H_2O$), lead nitrate ($Pb(NO_3)_2$), cadmium chloride ($CdCl_2$), and anhydrous chromium chloride ($CrCl_3$) were utilized to prepare metal solutions for the adsorption experiments. The media's and other solutions' pH was adjusted using HCl and NaOH.

2.2. Biochar Production Uses Camel Manure

Camel excrement was collected from a camel farm located near Sharourah, which is in the Najran area of Saudi Arabia. After the plant particles were removed, the manure was dried in the air. The dung was dried in the oven for 48 hours at a temperature of 60˚C. Camel dung was converted into biochar by subjecting it to slow pyrolysis in an electrical muffle furnace at 500˚C for 4 hours in an oxygen-free atmosphere. The charcoal cooled down overnight in the container by free convection. The selected fraction was kept in airtight containers until it was tested after the biochar was sieved to a size of 0.6 to 1.4 mm [28].

2.3. Synthesis of Biochar/Fe_3O_4 Nanocomposite

The biochar/Fe_3O_4 nanocomposite was synthesized by dissolving 2 g of iron chloride hexahydrate ($FeCl_3 \cdot 6H_2O$) in 100 mL of distilled water, adding 3 g of biochar to a 250 mL beaker, and mechanically stirring at 250 rpm for 2 hours forming the biochar/Fe_2O_3 nanocomposite. The mixture had been heating on an 80˚C hot plate for 3 hours. The reaction pH was 8.5. Nanocomposite production was confirmed by liquid color change for dark brown color. Biochar/Fe_2O_3 nanocomposite was

isolated from solution by centrifugation at 4000 rpm for 30 minutes after reaction. The biochar/Fe_2O_3 nanocomposite powder has been incubated at 400˚C for two hours. Dry material was powdered and calcined at 600˚C for two hours in an open-air furnace.

2.4. Physio-Chemical Characterizations of Biochar/Fe_3O_4 Nanocomposite

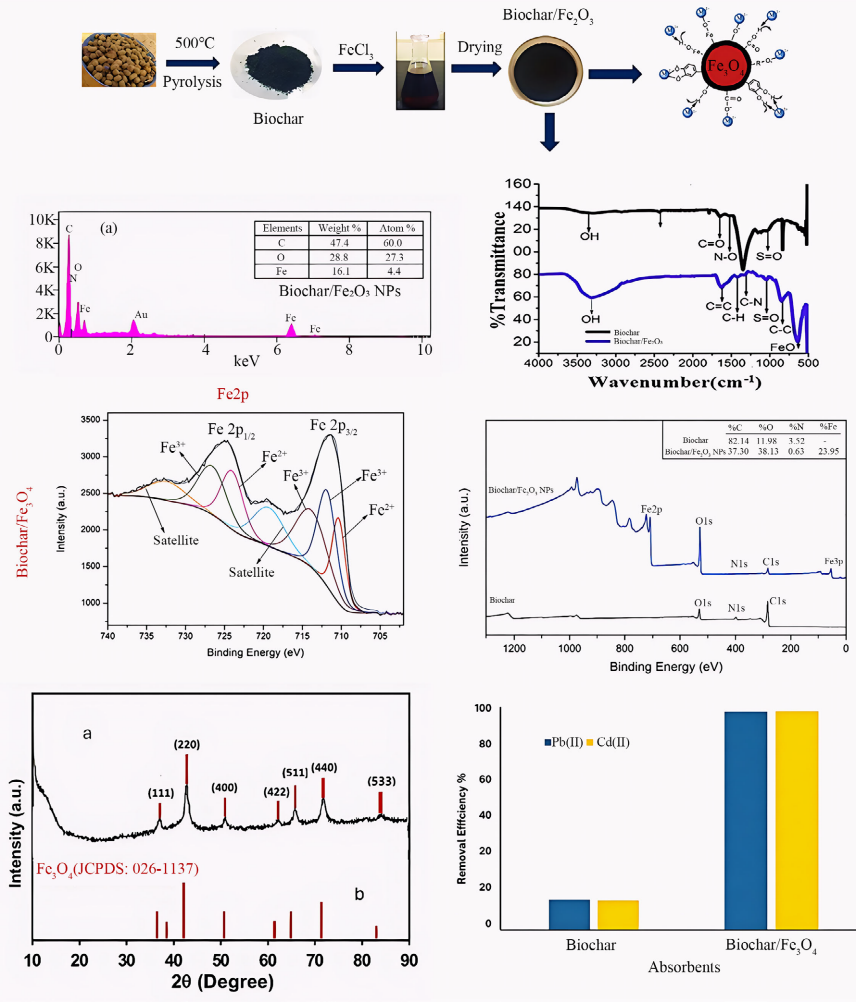

Figure 1. The schematic synthesis of biochar/Fe_2O_3 nanocomposite.

The biochar/Fe_3O_4 nanocomposite was studied using several analytical methods, including SEM, FTIR, BET, EDX, TGA, and XRD. FTIR analysis (range 500 - 4000 cm^{-1}) was used to identify the biomolecules that were responsible for the reduction, stabilization, and capping of the biochar/Fe_3O_4 nanocomposite. FTIR spectrum analysis was done using Origin Pro 8.5 software. SEM was used to determine the size and surface appearance of the biochar/Fe_3O_4 nanocomposite. Important information regarding the NPs' physical characteristics was revealed by this method. The biochar/Fe_3O_4 nanocomposite was analyzed using EDX to determine the presence of Fe and other elements. The EDX data revealed the atomic content

of the produced NPs, which reflected their atomic structure. Data were recorded over 2θ range of 20 - 80 with a step increment of 0.02 and interval time of 0.008 s per step. Surface morphology and composition on the surface were visualized and determined using Scanning Electron Microscopy-Energy Dispersive X-ray Spectroscopy (SEM-EDX, Thermos Scientific, US, SU-70). X-ray diffractometer XRD analysis was performed to verify the quality of the biochar/Fe_2O_3 nanocomposite. The TGA analysis used measurement of the weight loss during defined temperature for biochar/Fe_3O_4 nanocomposite. Using the Scherrer equation, the average crystalline size of the produced iron oxide nanoparticle. To find the zeta potential of each biochar and biochar/Fe_3O_4, a 0.002 g sample was dissolved in 25 milliliters of Milli Q water. Using 0.1 M NaOH and 0.1 M HCl, the suspension pH was brought within the range of 2 to 10. The suspensions were ultrasonically distributed for three hours at 25˚C in a bath-type sonicator. The Zetasizer Nano ZS90, Malvern, UK's JS94G+ micro electrophoresis device was used to test the electrophoresis mobility (**Figure 1**).

2.5. Batch Adsorption Experiments

The biochar/Fe_3O_4 nanocomposite was used as the adsorbent in the adsorption studies, and the adsorbate was Pb, and Cd ions. Within a 250 ml conical flask, 0.5 gramme of the adsorbent was dissolved in 100 ml of an aqueous solution that included metal ions at a concentration of 100 mg/l. The present study examined the effects of several variables on the adsorption of Cd, Pb ions, including pH (varying from 2 to 10), starting metal ion concentration (10 - 100 mg/l), and contact period (10 - 120 minutes). An orbital shaker was used to stir the mixture of adsorbents and adsorbate at 150 rpm for a predetermined amount of time at room temperature. Whatman-40 filter paper was used to filter the mixture, and a Flame Atomic Adsorption Spectrometer (FAAS) SHIMADZU AAS AA-7000, Japan, was used to measure the initial and final metal concentrations in the filtrate. The percentage removal efficiency and the capacity for adsorption of each metal ion by the biochar/Fe_2O_3 nanocomposite have been calculated, as indicated in Equation (1) and Equation (2) [29].

$$q_e = \frac{\left(C_i - C_e\right)}{W} xV \tag{1}$$

$$R(\%) = \frac{\left(C_o - C_e\right)}{C_i} x \tag{2}$$

The starting and equilibrium concentrations of metal ions after a time, t, are denoted as C_i (mg/L) and C_e (mg/L), respectively. V stands for the volume of the metal ion solution (L), W for the mass of the biochar/Fe_2O_3 nanocomposite used (g), and q_e for the mass of metal ions adsorbed onto the biochar both at equilibrium and after time t.

The pseudo-first- and pseudo-second-order models, which provide mathematical frameworks to comprehend the temporal elements of the adsorption process,

were used to investigate adsorption kinetics. The initial adsorption rate and rate constant are estimated via the pseudo-first-order model, which mostly concentrates on early-stage behavior. The pseudo-second order model, however, assumes that the adsorption rate and empty sites are proportionate. A more thorough knowledge of the whole adsorption process, including rate constants and maximum adsorption capacities, is offered by the pseudo-second order model.

The equations of the pseudo-first-order model may be found in Equation (3).

$$q_t = q_e\left(1 - e^{-k_1 t}\right) \tag{3}$$

The pseudo-second-order model is expressed in its nonlinear form as:

$$q_t = \frac{q_{e^2} k_2 t}{1 + q_e k_e t} \tag{4}$$

After the solid adsorbent was washed with water, the desorbed concentrations of the metal ions were analyzed to investigate the leaching of Pb(III) and Cd(II) ions. Following that, Pb(III) and Cd(II) were repeatedly removed using the regenerated adsorbent, and the corresponding removal efficiencies were evaluated at the second run.

3. Results and Discussion

3.1. Characterization of Biochar/Fe_3O_4

Figure 2 shows the results of an FTIR analysis of biochar made from camel manure and biochar/Fe_3O_4 nanocomposite. This analysis compared the functional groups in the biochar and those linked to the biochar/Fe_3O_4 nanocomposite that might aid in the adsorption of heavy metals. Many noticeable peaks were seen in the biochar spectra at wavenumbers 3325, 2931, 1777, 1642, and 1038 cm^{-1}. The presence of the O-H at about 3325 cm^{-1} supports the presence of alcohols, carboxyl, and phenols in biochar because of the presence of lignin and hemicellulose [30]. It also shows the presence of the broad peak of O-H stretching. The alkyl's -C-H stretch in biochar is represented by the band at 2931 cm^{-1}. There is probably a C=O (carbonyl) present, which is the cause of the broad peak seen at about 1677 cm^{-1}. The peak at 1690 - 1380 is explained by C=O stretching, which is frequently found in carboxyl and ketone compounds, as well as C=C vibrations in aromatic rings. According to [31], the sulfoxide group (S=O) is represented by the peak at 1034 cm^{-1}. Like this, the biochar/Fe_3O_4 nanocomposite's FTIR spectra shows clear peaks. A peak was detected at 3321 cm^{-1}, indicating the presence of an O-H functional group. In alkenes, a noticeable peak at 1632 cm^{-1} that is connected to the C=C stretching vibration was noted. As previously reported [32], the presence of the C-H stretching mode in asymmetric and symmetric aliphatic and aromatic hydrocarbons was also suggested by the identification of a prominent peak at 1450 cm^{-1}. Sulfur oxide and hydroxyl groups were detected in the biochar/Fe_3O_4 nanocomposite by FTIR analysis, as indicated by separate peaks at 1051 and 3321 cm^{-1}, respectively. These results imply the production of a biochar/Fe_3O_4 nanocompo-

site and the reduction of Fe^{3+} ions; the absorption band at 631 cm^{-1} offers compelling proof of the successful establishment of Fe-O bonds. Previous research on the FTIR spectroscopy of biosynthesized iron oxide nanoparticles has found absorption bands at wavelengths like 618 [33] and 630 [34], which is in line with our findings. The surface charge of biochar was measured using zeta potential values as a function of pH, as shown in **Figure 3**. As may be seen, the sites of zero charge for biochar and biochar/Fe_3O_4 are 3.2 and 3.7, respectively. Biochar/Fe_3O_4 has a greater pHPZC value than biochar, which may be explained by the impregnation of Fe_3O_4, which has a pHPZC value of 5 [35]. Higher temperature-produced biochar often has less negative charges because it lacked acidic functional groups [36]. Biochar/Fe_3O_4 showed the highest potential for electrostatic adsorption and the highest negative surface charges in the pH 2 - 10 range [37] [38].

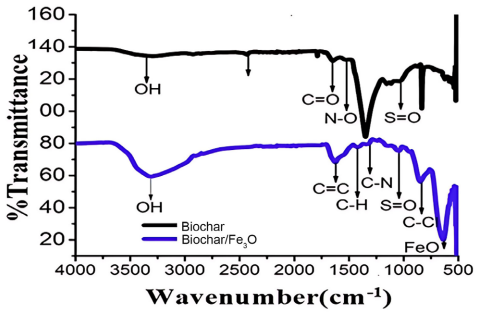

Figure 2. FT-IR spectra of camel manure-derived biochar and biochar/Fe_3O_4 nanocomposite, illustrating surface functional groups and Fe-O bond formation.

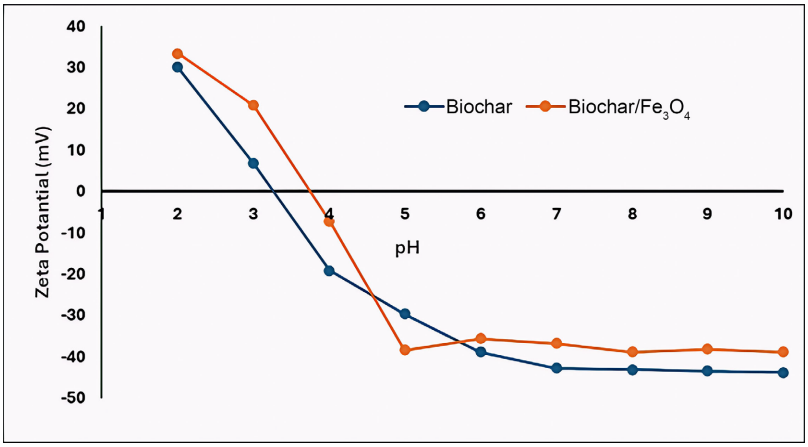

Figure 3. Zeta potential of biochar and biochar/Fe_3O_4 as a function of solution pH, indicating the point of zero charge and surface charge behavior.

The phase purity and crystallinity of the biochar/Fe_3O_4 nanocomposite can be discerned through XRD analysis. The research demonstrated consistent XRD patterns of the biochar/Fe_3O_4 nanocomposite, which utilized biochar nanoparticles [28]. The diffraction peaks of the synthesized Fe_3O_4-NPs, as illustrated in **Figure 4**, were observed at 2θ values of 36.57˚, 43.47˚, 54.52˚, 61.25˚, 63.74˚, 71.91˚, and 84.66˚. These peaks correspond to the crystal planes designated as (111), (200),

(311), (400), (422), (511), (440), and (533), respectively. In contrast, several distinct phase peaks were noted within the 2θ range of 30˚ - 90˚ as illustrated in Figure 4, suggesting the extent of crystallinity in the phases observed in the two biochars. The observed weak diffraction peak at 36.57˚ may be ascribed to the presence of amorphous carbon [39]. The diffraction peaks under analysis exhibited a strong correlation with the standard XRD patterns of magnetite (Fe_3O_4), as referenced by JCPDS file no: 00-026-1137, confirming the cubic crystallographic system.

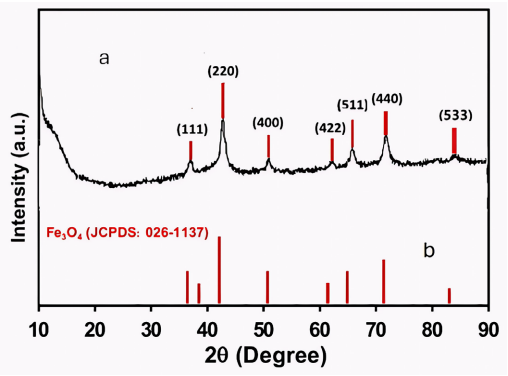

Figure 4. XRD patterns of biochar/Fe_3O_4 nanocomposite.

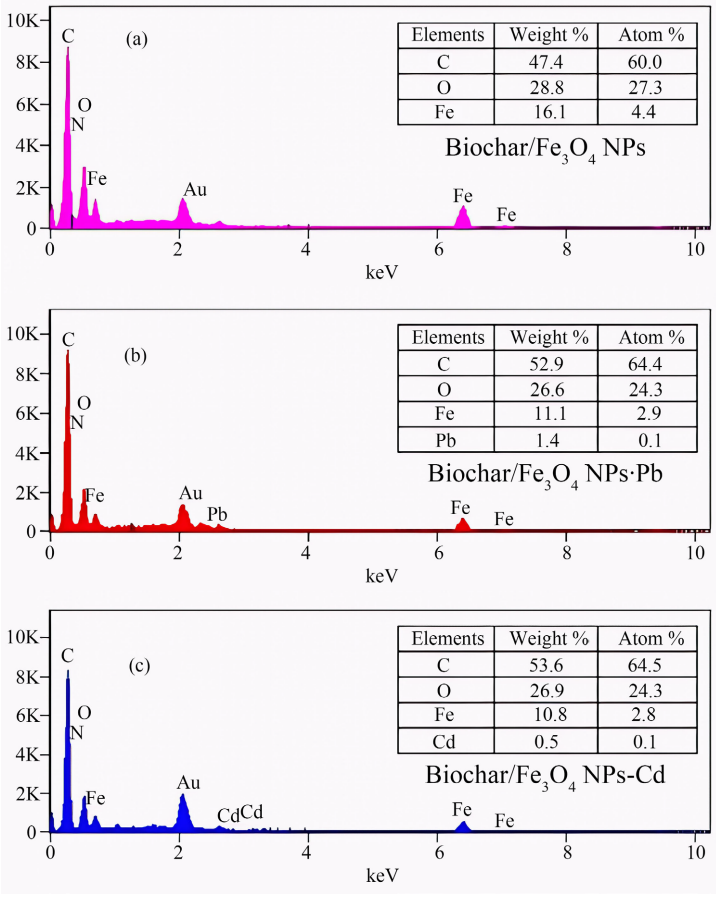

Figure 5. EDX results of biochar/Fe_3O_4 nanocomposite before (A) and after adsorption of Pb (B) and Cd (C).

SEM-EDX analyses were performed to get a better understanding of the chemical structure of the biochar/Fe_3O_4 nanocomposite after the adsorption process. The goal of these analyses was to uncover the processes of adsorption for Pb(II) and Cd(II). First, as shown in Figure 5, clear peaks of Pb(II) and Cd(II) were observed in the EDX spectra after the adsorption process. At the same time, the peak intensity of iron decreased noticeably, which confirmed that Pb(II) and Cd(II) were successfully adsorbed onto the biochar/Fe_3O_4 nanocomposite. At the same time, the iron components played a significant role in the adsorption process [40]. A technique known as elemental mapping was used to confirm the existence of elements and their distribution throughout the biochar/Fe_3O_4 nanocomposite. Figure 6 demonstrates that the primary elements (C, O, Fe, and Pb/Cd) in the structure of the biochar/Fe_3O_4 nanocomposite were distributed uniformly and continuously over the surface of the biochar/Fe_3O_4 nanocomposite after adsorption. This indicates that the structure of the nanocomposites remained stable throughout the adoption process.

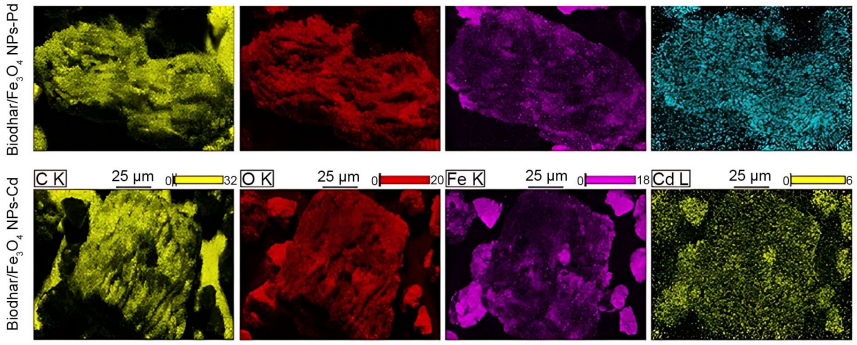

Figure 6. Element mapping analysis of biochar/Fe_3O_4 nanocomposite after adsorption of Pb and Cd.

3.2. The Analysis of X-Ray Photoelectron Spectroscopy (XPS)

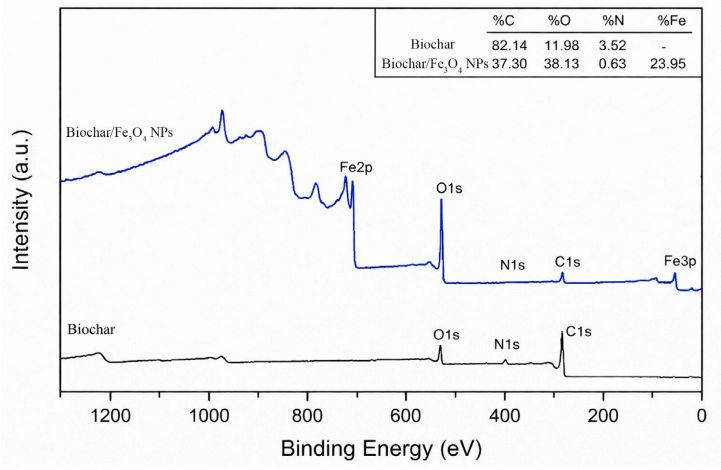

Figure 7. XPS spectrum of each biochar and biochar/Fe_3O_4 NPs.

The magnetic nanocomposites' oxidation state and elemental makeup were ascer-

tained using XPS. The total XPS spectra of the magnetic biochar and biochar produced using the method are shown in Figure 7. The biochar's C1s and O1s bonds, which demonstrate the existence of carbon and oxygen, can be seen. Due to the Fe-O interaction of the Fe_3O_4 nanoparticles, separate Fe ($3p_{3/2}$), Fe ($2p_{3/2}$), and Fe ($2p_{1/2}$) bonds were observed in the spectra of biochar/Fe_3O_4 NPs at about 54, 712, and 725 eV [41]. The inset table (Figure 6) demonstrates that after iron impregnation in biochar/Fe_3O_4 NPs, the atomic percentage of C significantly dropped while the O% significantly rose. Because the organic materials in camel manure-derived biochar are capping onto iron oxide nanoparticles, the surface of biochar/Fe_3O_4 NPs has a greater C content but a lower O and Fe content, which is compatible with the EDX findings.

The C1s and O1s XPS spectra of biochar are shown in Figure 8(a). The C1s spectra of biochar was deconvoluted into five main peaks, which correspond to carbide (282.5 eV), C-H (283.6), C-C/C=C (284.2 eV), C-O-C (286.6 eV), and C=O (288.7 eV), as shown in Figure 8(b) and Table 1 [42]. After being magnetized using a certain method, the components of biochar underwent a transformation. The carbon and C-H bond at peaks about 282 eV in the C1s spectra of biochar/Fe_3O_4 were ascribed to the carbon, whose intensity dramatically increased after the successful impregnation of iron oxide using the co-precipitation approach [43]. The presence of various functional groups on the biochar/Fe_3O_4 surface in the C1s spectrum is confirmed by XPS spectra, which are linked to elemental analysis and FTIR analysis [44]. Additionally, the proportion of oxygen-containing functional groups in biochar/Fe_3O_4 is higher, confirming the surface functionalization of the co-precipitation method.

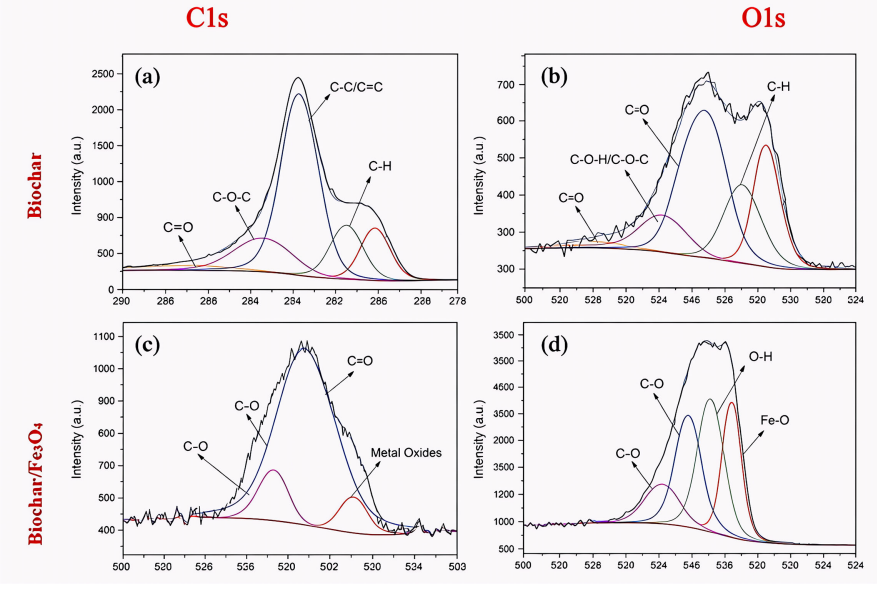

Figure 8. Biochar and Biochar/Fe_3O_4 NPs' C1s and O1s deconvolution.

Metal oxides in biochar are responsible for the binding energy in the O1s region between 529.1 eV and 530.71 eV [45]. K_2O, CaO, MgO, and other metal oxides

may be present in biochar [46] (**Table 2**). Because so much iron is added, the linkages in biochar/Fe_3O_4 are mostly inorganic oxygen bound to iron (FeO, Fe_2O_3, Fe_3O_4) [43]. According to the FTIR data, the newly observed signal at 532 eV in biochar/Fe_3O_4 was ascribed to -OH or molecular water, which mostly originated from moisture.

Table 1. Information of structure and binding energy values of the prepared biochar and biochar/Fe_3O_4 NPs.

Peaks	Biochar			Biochar/Fe_3O_4		
	Structure	BE (eV)	%At	Structure	BE (eV)	%At
C1s	Carbide	282.39	13.89	Carbide	282.14	25.14
	C-H	283.71	15.21	C-H	282.98	31.01
	C-C/C=C	285.11	53.21	C-C/C=C	284.11	40.04
	C-O-C	286.42	14.37	C-O-H/C-O-C	285.61	13.39
	C=O	289.33	4.19	C-N	286.36	6.02
				C=O	287.91	2.40
O1s	Metal oxides	529.11	7.10	Fe-O	530.91	25.20
	C=O	531.13	82.01	O-H	531.97	32.98
	C-O	533.39	10.89	C=O	533.11	31.08
Fe $2p_{3/2}$				C-O	534.23	11.74
				Fe^{2+}/Fe_3O_4	710.41	13.24
				Fe^{2+}/Fe_3O_4	712.08	19.36
					714.12	19.87
Fe $2p_{1/2}$				Satellite peak	719.86	12.9
				Fe^{2+}/Fe_3O_4	724.15	15.01
				Fe^{2+}/Fe_3O_4	727.99	10.12
				Satellite peak	733.14	9.49
				Fe^{2+}/Fe_3O_4 ratio	0.572	

Figure 9 displays the Fe 2p spectra, and **Table 1** provides a summary of the data for each deconvoluted peak. Seven peaks were found in the deconvoluted Fe 2p spectra of biochar/Fe_3O_4, and they are shown in **Figure 9**. $2p_{3/2}$ and $2p_{1/2}$ of Fe^{3+}cwere represented by the three spectral bands at 712.7 eV, and 727.99eV, respectively. Fe^{2+} species $2p_{3/2}$ and $2p_{1/2}$ may be responsible for the other two peaks, which had binding energy levels of 710.34 eV and 724.15 eV, respectively. combined with the last two peaks, which were matching peaks of Fe^{3+} and Fe^{2+} at 719.87eV and 732.9 eV, respectively, showing that the Fe_3O_4 phase in biochar/Fe_3O_4 was successfully formed [47]. Given that $FeO{\cdot}Fe_2O_3$ is another way to define stoichiometric Fe_3O_4, the Fe^{2+}/Fe^{3+} ratio ought to be 1/2 [48]. The deconvoluted satellite peaks of 0.572 in this study's Fe^{2+}/Fe^{3+} findings show that the co-precipitation process generated pure Fe_3O_4.

Table 2. Metal contents in biochar and biochar/Fe_3O_4 (mg/g).

	Biochar	Biochar/Fe_3O_4
Fe	0.5318	385.2011
Al	0.3850	0.0289
Ca	10.1542	3.1859
Na	0	0.3098
Mg	3.0393	1.1406
K	9.8171	0.3406
Si	0.2011	0.3611

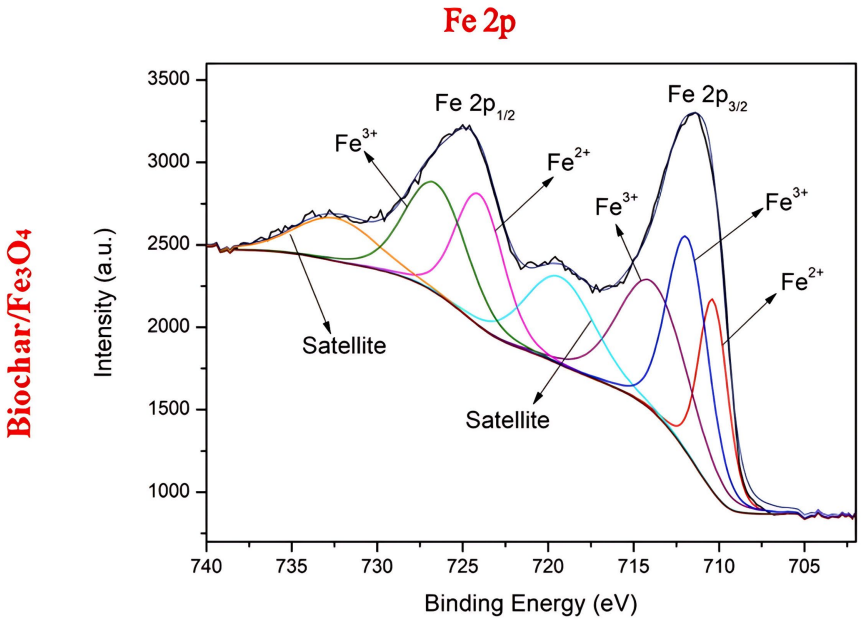

Figure 9. Deconvolution of Fe 2p of the biochar/Fe_3O_4.

3.3. The pH Effect on Lead and Cadmium Adsorption

One of the most important factors affecting the surface charge and dissociation of functional groups on the adsorbent during the adsorption process is the pH of the solution. Moreover, the degree of ionization and speciation of the metal ions is also influenced by the pH of the solution [49]. The adsorptive removal of both Pb(II) and Cd(II) from the aqueous solution was evidently pH-dependent, as shown in **Figure 10(a)**, **Figure 10(b)**. This suggests that the adsorption was strongly connected to the electrostatic forces between Pb(II)/Cd(II) and biochar/Fe_3O_4 [50] [51].

For Pb(II) and Cd(II) recovery, the biochar/Fe_3O_4 outperformed the biochar in almost the whole pH range investigated. In the case of Pb(II), for example, both biochar and biochar/Fe_3O_4 removal percentages were low (pH 2), but for biochar/Fe_3O_4, the percentage removal increased dramatically from pH 2 to pH 6 and reached equilibrium, which was 96.2% at pH 6. However, the amount of Pb(II)

removed from biochar only slightly increased (from 1.6% to almost 16.2%). At pH 2, biochar and biochar/Fe_3O_4 showed the least amount of Cd(II) elimination. But with biochar/Fe_3O_4, removal increased from as low as 2.1% to almost 68.4% as pH increased from 2 to 4, reaching a maximum removal efficiency of 92.82% at equilibrium pH 6.

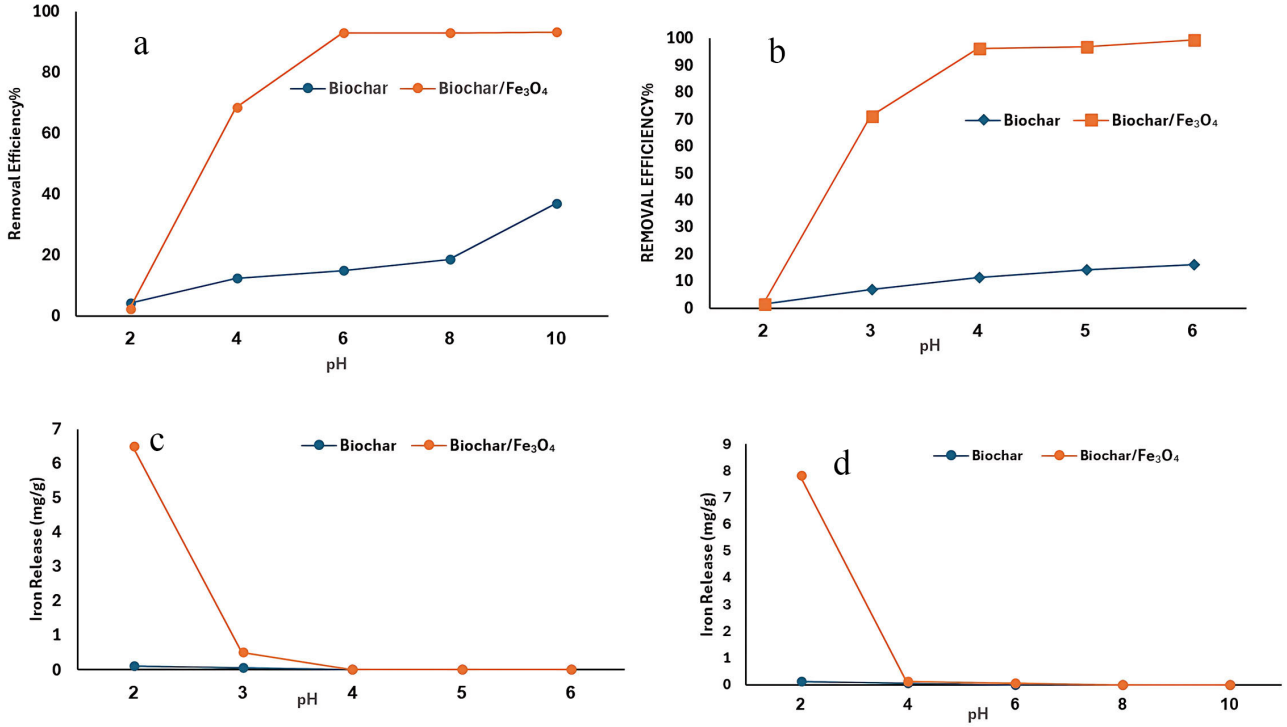

Figure 10. Effect of initial solution pH on Pb(II) and Cd(II) removal efficiency and corresponding iron leaching behavior of biochar/Fe_3O_4.

The removal of Cd(II) on biochar exhibited a modest increase of 14.18% as the pH shifted from 2 to 8, which stands in contrast to the findings related to Pb(II). At pH 10, a notable increase in Cd(II) removal was observed for both types of biochar, likely due to the precipitation of $Cd(OH)_2$. The limited adsorptive removal observed at low pH can be attributed to the elevated concentration of H+ ions in the solution. These ions compete with Pb(II) and Cd(II) for bonding with the active sites of biochar [52]. This competition leads to the saturation of the bonded active sites, making them unavailable for interaction with other cations. The results of the zeta potential analysis indicated that biochar exhibited a pH of 3.18. These ions compete with Pb(II) and Cd(II) for bonding with the active sites of biochar, leading to the saturation of these sites and making them unavailable for interaction with other cations. The rise in pH led to a decrease in H+ concentration, and the deprotonation of functional groups on the biochar surface resulted in a shift from a positive to a negative surface charge. This change enhanced the adsorption of Pb(II) and Cd(II) onto the biochar (**Figure 3**). In addition to the acidic functional groups such as phenolic, hydroxyl, and carboxylic acid that are

anchored on the surface of biochar, iron oxides are capable of forming iron hydroxide complexes in aqueous solution [53].

The stability of magnetic biochar was assessed by investigating the leaching of Fe ions from biochar/Fe_3O_4 during adsorption experiments with Pb(II) and Cd(II) across various pH levels. **Figure 10(c)** and **Figure 10(d)** illustrate that the leaching of iron exhibited a consistent pattern for both Pb(II) and Cd(II), characterized by a rapid decrease from pH 2 to pH 4, while the loss remained minimal beyond pH 4. At a pH of 2, the quantity of iron extracted from biochar/Fe3O4 was measured at 6.62 mg/g in Pb(II) solutions and 7.62 mg/g in Cd(II) solutions. Considering the findings and the results regarding the effect of pH on sorption, pH 5 was selected for both Pb(II) and Cd(II) for the subsequent experiments discussed below.

3.4. Adsorbent Dosage's Effects on Lead and Cadmium Adsorption

Evaluation of the effect of adsorbent dose on Pb(II) and Cd(II) adsorption revealed that removal efficiency for both Pb(II) and Cd(II) rose as adsorbent dosage increased (**Figure 11**). With practically all the Pb(II) and Cd(II) eliminated, the removal efficiency remained essentially the same with adsorption dosages of 4 g/L for Pb(II) and 6 g/L for Cd(II). The concentration of residual metal ions in the solution is large when the absorbent surface is saturated with metal ions at low adsorbent dosages. As the dose of the adsorbent was raised, the removal of metal ions increased as well, until the concentrations of surface and solution metal ions balanced out. But when the dose of the adsorbent increased, the quantity of metal ions that biochar was able to absorb per unit mass dropped significantly. The dose was set at 2 g/L and 4 g/L for Pb(II) and Cd(II) adsorption tests in the ensuing experiments to achieve high removal efficiency and to fully use the biochar.

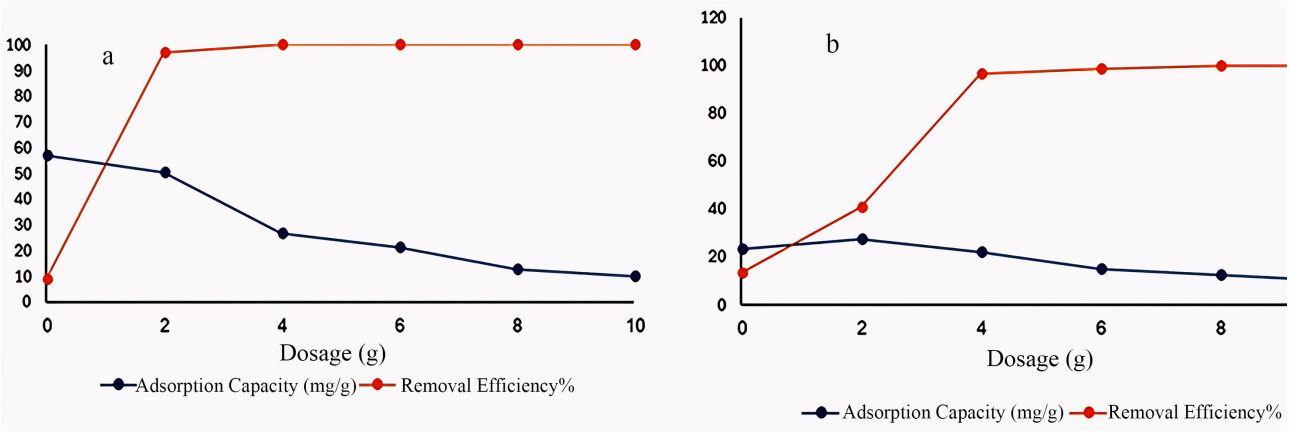

Figure 11. Effect of dose on (a) Pb(II) and (b) Cd(II) adsorption on biochar/Fe_3O_4 (pH = 5, starting concentration = 100 mg/L, contact period = 24 hours).

3.5. Kinetics Studies of Lead and Cadmium

The pseudo first-order and pseudo second-order kinetic models were used to ex-

amine experimental data to further assess the adsorption efficiency (Figure 12). To study the effect of contact duration on Pb(II) and Cd(II), we used a starting concentration of 100 mg/L at pH 5, as shown in Figure 12. There are two noticeable steps to the adsorption kinetics of Pb(II) and Cd(II): the first is a fast uptake, and the second is a gradual uptake. One possible explanation is that the biochar/Fe_3O_4 nanocomposite gradually becomes saturated with the available active sites over time, making it difficult for Pb(II)/Cd(II) to be adsorbed onto the biochar. Biochar exhibited a delayed adsorption of Pb(II)/Cd(II) because, whereas 91% removal efficiency for Pb(II) was achieved within 30 minutes, 91% sorption of Cd(II) happened about 4 hours, leading to an adsorption of around 42% and a tendency to become more saturated with time. Adsorption of roughly 43 mg/g for Pb(II) and 27 mg/g for Cd(II), respectively, were achieved after 30 minutes and 4 hours, respectively, according to the corresponding removal efficiencies. The adsorption capacities of Pb(II) (46.33 ± 0.25 mg/g) and Cd(II) (28.51 ± 0.41 mg/g) did not show any notable improvement after 4 hours and 24 hours, respectively. Thus, it can be inferred that, given the experimental circumstances utilized, biochar/Fe_3O_4 has a higher speed and capacity adsorption affinity for Pb(II) compared to Cd(II).

The experimental results for both metal ion solutions more closely fit the pseudo-second-order model than the pseudo-first-order model, according to the comparison of R^2 values, which is shown in Table 3. The strong agreement between the measured q_e and the anticipated q_e values for both Pb(II) and Cd(II) ions adsorbed over biochar/Fe_3O_4 further supports the validity of the pseudo-second-order model. These results are consistent with previous research that has shown that pseudo-second-order adsorption kinetics may be applied to Pb(II) and Cd(II) adsorption onto biochar made from plant and/or animal biomass [54]-[56].

Pseudo-second-order kinetics show that chemisorption controls adsorption or that metal ions and biochar/Fe_3O_4 share electrons [56]. Its shows biochar/Fe_3O_4 may effectively adsorb these metal ions, making it an intriguing candidate for aqueous solution contamination removal.

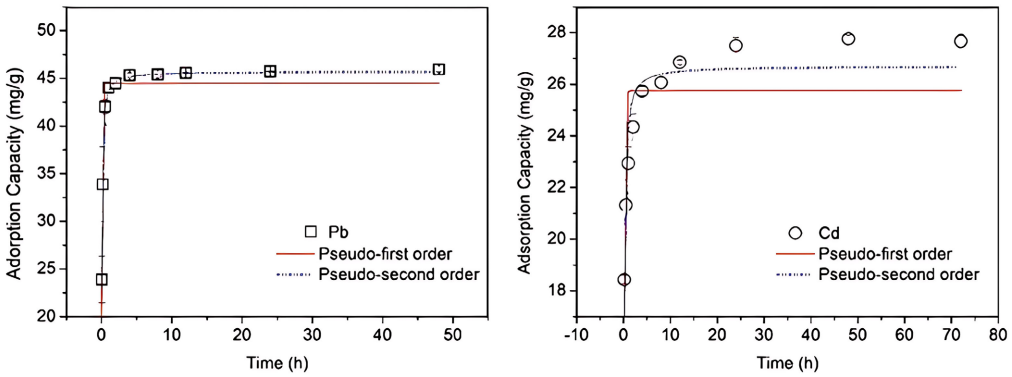

Figure 12. Pb(II) and Cd(II) adsorption kinetics and isotherm on biochar/Fe_3O_4 (pH = 5, starting concentration = 100 mg/L, dosage = 2 g/L for Pb, 4 g/L for Cd).

Table 3. Adsorption Kinetics Parameters for Pb(II) and Cd(II) onto biochar/Fe_3O_4.

Matel ion	Pseudo-first order model		Pseudo-second order model	
Pb(II)	k_1 (1/min)	10.9543	k_2 (g/mg min)	0.5468
	q_e (mg/g) (cal)	29.6580	q_e (mg/g) (cal)	45.1765
	q_e (mg/g) (exp)	45.6625	q_e (mg/g) (exp)	46.7698
	R^2	0.8537	R^2	0.9875
Cd(II)	k_1 (1/min)	1.7675	k_2 (g/mg min))	0.0437
	q_e (mg/g) (cal)	6.9872	q_e (mg/g) (cal)	26.7641
	q_e (mg/g) (exp)	26.8765	q_e (mg/g) (exp)	27.3421
	R^2	0.7943	R^2	0.9923

3.6. Adsorption Study for Cadmium and Lead

To get a fundamental grasp of the removal capabilities of the adsorbent created in this study, the removal efficacy of different adsorbents was investigated utilizing Pb(II) and Cd(II) ions as the adsorbates. Figure 13 compares the removal efficacy of biochar derived from camel dung with biochar/Fe_3O_4 nanoparticles. Pb(II) ion removal on biochar was 12.25%, while Cd(II) ion removal was 10.67%. Biochar/Fe_3O_4 demonstrated a higher ability to remove both metal ions than biochar derived from camel dung, and co-precipitation magnetization enhanced Pb(II) and Cd(II) uptake overall. The biochar/Fe_3O_4 demonstrated an exceptionally high removal efficiency for both Pb(II) (97.46%) and Cd(II) (99.17%) ions under the experimental circumstances, which were almost completely adsorbed by the material. This suggests that biochar/Fe_3O_4 has a significant deal of promise for heavy metal removal from aqueous solution.

3.7. Stability of Biochar/Fe_3O_4

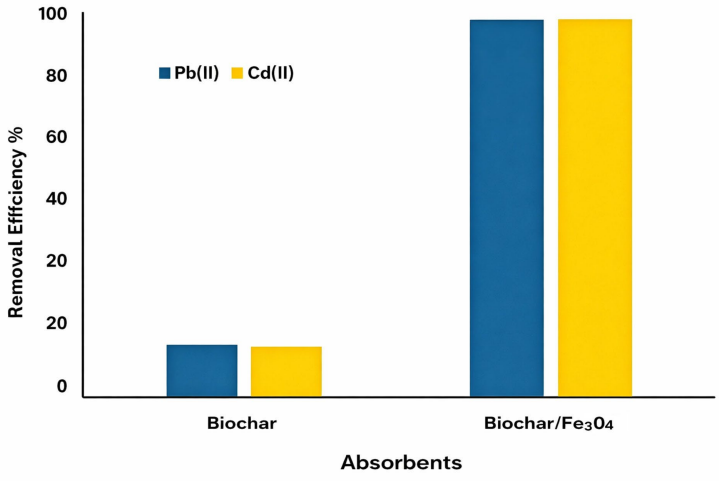

Figure 13. Comparison of biochar and biochar/Fe_3O_4 nanoparticles for Pb(II) and Cd(II) (Initial concentration: 100 mg/L, Dosage: 4 g/L, pH = 6.0) adsorption.

The stability of magnetic biochar was assessed by investigating the leaching of iron

from biochar/Fe_3O_4 nanoparticles within a pH range of 2 to 6. Figure 14 illustrates that the leaching of iron exhibited a consistent pattern, with a significant decrease occurring from pH 2 to pH 3, followed by negligible loss beyond pH 3 for biochar/Fe_3O_4 nanoparticles. At a pH of 2.0, the quantity of iron released from biochar/Fe_3O_4 was measured at 5.92 mg/g. The increased leaching amount in biochar/Fe_3O_4 can be attributed to the reduced iron content in biochar/Fe_3O_4. Approximately 0.3 mg/g of iron was still released from biochar/Fe_3O_4 at pH 3. Consequently, the biochar/Fe_3O_4 demonstrates greater stability under acidic conditions.

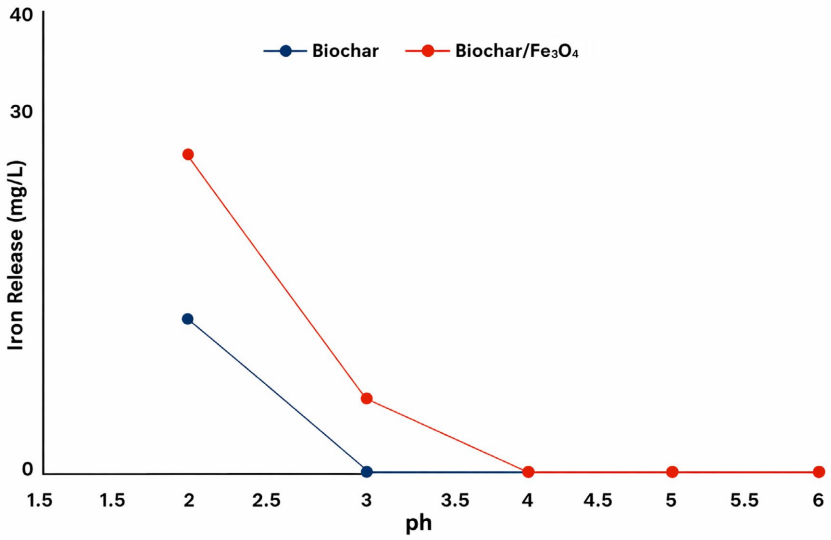

Figure 14. Leaching of iron of biochar/Fe_3O_4.

3.8. Potential Adsorption Mechanisms

The results indicated that the surface functional groups of biochar/Fe_3O_4 nanoparticles experienced qualitative alterations before and during adsorption. Moreover, it was apparent that the hydroxyl and carboxyl groups, along with triple bonds or accumulated double bonds, and the incorporation of Fe_3O_4 particles were predominantly consumed during the adsorption of Pb(II) and Cd(II) to create inner complexes (-COO-M, -O-M, C:M^{2+}, and Fe-O-M, where M represents Pb or Cd), resulting in the attenuation or displacement of the characteristic bands of COOH, O-H, and Fe-O. Additionally, co-precipitation happened to generate the basic $PbCO_3$ component during the adsorption process, which aligned well with the results from the XRD study.

The SEM-EDX, XRD, and FTIR results allow us to suggest some possible ways that Pb(II) and Cd(II) might stick to the surface of biochar/Fe_3O_4 nanoparticles. Some potential adsorption processes of Pb(II) and Cd(II) on the surface of biochar/Fe_3O_4 nanoparticles may be suggested based on the results of SEM-EDX, XRD, and FTIR investigations.

First, the strong electrostatic attraction between the negatively charged functional

groups, such -COO- and -OH-, on the surface of biochar/Fe_3O_4 nanoparticles and the positively charged Pb(II) and Cd(II) seen in Figure 15 illustrates the importance of the bonding process. Second, since iron oxides have a strong affinity for lead and cadmium, they are crucial to the adsorption of Pb(II) and Cd(II) by biochar/Fe_3O_4 nanoparticles. Finally, the adsorption of Pb(II) onto biochar/Fe_3O_4 nanoparticles may be improved by the co-precipitation of Pb(II) on the surface of the nanoparticles.

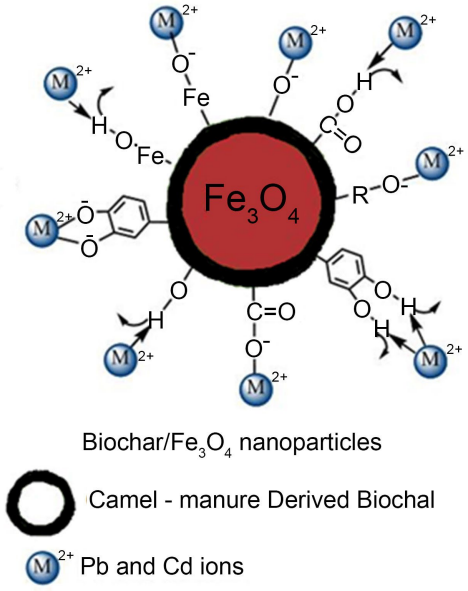

Figure 15. Potential adsorption mechanisms of biochar/Fe_3O_4 nanoparticles.

4. Conclusion

In this study, camel manure-derived Biochar and iron oxide (Biochar/Fe_3O_4) nanoparticles were synthesized and used as an effective adsorbent for the removal of Pb(II) and Cd(II) from wastewater. The effectiveness of Biochar/Fe_3O_4 in biosorption is influenced by factors such as time, pH, and the quantity of absorbent used. The pseudo-first and second-order kinetic models for the biosorption of Pb(II) and Cd(II) were applied to Biochar/Fe_3O_4 nanoparticles. The results obtained from these models demonstrate strong homogeneity, highlighting the significant potential of these nanopastes. Furthermore, the adsorption mechanism was found to be predominantly chemical in nature, indicating their promising applicability in both environmental sustainability and industrial applications. The findings suggest that Biochar/Fe_3O_4 nanoparticles may serve as a viable alternative for the efficient and rapid removal of Pb(II) and Cd(II).

Conflicts of Interest

The authors declare no conflicts of interest regarding the publication of this paper.

References

[1] Ali, H., Khan, E. and Ilahi, I. (2019) Environmental Chemistry and Ecotoxicology of

Hazardous Heavy Metals: Environmental Persistence, Toxicity, and Bioaccumulation. *Journal of Chemistry*, **2019**, Article ID: 6730305. https://doi.org/10.1155/2019/6730305

[2] Mishra, S., Bharagava, R.N., More, N., Yadav, A., Zainith, S., Mani, S., *et al.* (2018) Heavy Metal Contamination: An Alarming Threat to Environment and Human Health. In: Sobti, R., Arora, N. and Kothari, R. Eds., *Environmental Biotechnology: For Sustainable Future*, Springer, 103-125. https://doi.org/10.1007/978-981-10-7284-0_5

[3] Kour, J., Khanna, K., Bakshi, P., Sharma, I., Ohri, P., Mir, B.A., *et al.* (2020) Role of Beneficial Microbes in the Molecular Phytotoxicity of Heavy Metals. In: Faisal, M., Saquib, Q., Alatar, A.A. and Al-Khedhairy, A.A. Eds., *Nanotechnology in the Life Sciences*, Springer International Publishing, 227-262. https://doi.org/10.1007/978-3-030-45975-8_13

[4] Jaishankar, M., Tseten, T., Anbalagan, N., Mathew, B.B. and Beeregowda, K.N. (2014) Toxicity, Mechanism and Health Effects of Some Heavy Metals. *Interdisciplinary Toxicology*, **7**, 60-72. https://doi.org/10.2478/intox-2014-0009

[5] Ali, H. and Khan, E. (2019) Trophic Transfer, Bioaccumulation, and Biomagnification of Non-Essential Hazardous Heavy Metals and Metalloids in Food Chains/Webs—Concepts and Implications for Wildlife and Human Health. *Human and Ecological Risk Assessment: An International Journal*, **25**, 1353-1376. https://doi.org/10.1080/10807039.2018.1469398

[6] Genchi, G., Sinicropi, M.S., Lauria, G., Carocci, A. and Catalano, A. (2020) The Effects of Cadmium Toxicity. *International Journal of Environmental Research and Public Health*, **17**, Article 3782. https://doi.org/10.3390/ijerph17113782

[7] Knoell, D.L. and Wyatt, T.A. (2021) The Adverse Impact of Cadmium on Immune Function and Lung Host Defense. *Seminars in Cell & Developmental Biology*, **115**, 70-76. https://doi.org/10.1016/j.semcdb.2020.10.007

[8] Collin, M.S., Venkatraman, S.K., Vijayakumar, N., Kanimozhi, V., Arbaaz, S.M., Stacey, R.G.S., *et al.* (2022) Bioaccumulation of Lead (Pb) and Its Effects on Human: A Review. *Journal of Hazardous Materials Advances*, **7**, Article 100094. https://doi.org/10.1016/j.hazadv.2022.100094

[9] Nursidika, P., Kurnia, D. and Sugihartina, G. (2024) Elevated Blood Lead Levels in Women of Reproductive Age due to Leads Exposure from Contaminated Water. *Journal of Vocational Health Studies*, **7**, 175-180. https://doi.org/10.20473/jvhs.v7.i3.2024.175-180

[10] Chen, Q., Tang, Z., Li, H., Wu, M., Zhao, Q. and Pan, B. (2020) An Electron-Scale Comparative Study on the Adsorption of Six Divalent Heavy Metal Cations on $MnFe_2O_4$@CAC Hybrid: Experimental and DFT Investigations. *Chemical Engineering Journal*, **381**, Article 122656. https://doi.org/10.1016/j.cej.2019.122656

[11] Hama Aziz, K.H., Mustafa, F.S., Omer, K.M., Hama, S., Hamarawf, R.F. and Rahman, K.O. (2023) Heavy Metal Pollution in the Aquatic Environment: Efficient and Low-Cost Removal Approaches to Eliminate Their Toxicity: A Review. *RSC Advances*, **13**, 17595-17610. https://doi.org/10.1039/d3ra00723e

[12] Machado, A.A., Valiaparampil, J.G. and M, L. (2024) Unlocking the Potential of Algae for Heavy Metal Remediation. *Water, Air, & Soil Pollution*, **235**, Article No. 629. https://doi.org/10.1007/s11270-024-07436-3

[13] Kumar, D., Malyan, S.K., Kumar, A. and Kumar, J. (2021) Microbiological Removal of Heavy Metals from the Environment. In: Kumar, A. and Ram, C., Eds., *Nanobiotechnology for Green Environment*, CRC Press, 139-164.

https://doi.org/10.1201/9780367461362-6

[14] Limcharoensuk, T., Sooksawat, N., Sumarnrote, A., Awutpet, T., Kruatrachue, M., Pokethitiyook, P., *et al.* (2015) Bioaccumulation and Biosorption of Cd^{2+} and Zn^{2+} by Bacteria Isolated from a Zinc Mine in Thailand. *Ecotoxicology and Environmental Safety*, **122**, 322-330. https://doi.org/10.1016/j.ecoenv.2015.08.013

[15] Goyal, P. and Srivastava, S. (2009) Characterization of Novel Zea Mays Based Biomaterial Designed for Toxic Metals Biosorption. *Journal of Hazardous Materials*, **172**, 1206-1211. https://doi.org/10.1016/j.jhazmat.2009.07.125

[16] Lee, J.E. and Park, Y. (2020) Applications of Modified Biochar-Based Materials for the Removal of Environment Pollutants: A Mini Review. *Sustainability*, **12**, Article 6112. https://doi.org/10.3390/su12156112

[17] Zhang, P., Zhang, X., Yuan, X., Xie, R. and Han, L. (2021) Characteristics, Adsorption Behaviors, Cu(II) Adsorption Mechanisms by Cow Manure Biochar Derived at Various Pyrolysis Temperatures. *Bioresource Technology*, **331**, Article 125013. https://doi.org/10.1016/j.biortech.2021.125013

[18] Wei, D., Li, B., Huang, H., Luo, L., Zhang, J., Yang, Y., *et al.* (2018) Biochar-Based Functional Materials in the Purification of Agricultural Wastewater: Fabrication, Application and Future Research Needs. *Chemosphere*, **197**, 165-180. https://doi.org/10.1016/j.chemosphere.2017.12.193

[19] Masud, M.A.A., Shin, W.S., Sarker, A., Septian, A., Das, K., Deepo, D.M., *et al.* (2023) A Critical Review of Sustainable Application of Biochar for Green Remediation: Research Uncertainty and Future Directions. *Science of The Total Environment*, **904**, Article 166813. https://doi.org/10.1016/j.scitotenv.2023.166813

[20] Qin, J., Qian, S., Chen, Q., Chen, L., Yan, L. and Shen, G. (2019) Cow Manure-Derived Biochar: Its Catalytic Properties and Influential Factors. *Journal of Hazardous Materials*, **371**, 381-388. https://doi.org/10.1016/j.jhazmat.2019.03.024

[21] Xu, X., Cao, X., Zhao, L., Wang, H., Yu, H. and Gao, B. (2012) Removal of Cu, Zn, and Cd from Aqueous Solutions by the Dairy Manure-Derived Biochar. *Environmental Science and Pollution Research*, **20**, 358-368. https://doi.org/10.1007/s11356-012-0873-5

[22] Mohan, D., Sarswat, A., Ok, Y.S. and Pittman, C.U. (2014) Organic and Inorganic Contaminants Removal from Water with Biochar, a Renewable, Low Cost and Sustainable Adsorbent—A Critical Review. *Bioresource Technology*, **160**, 191-202. https://doi.org/10.1016/j.biortech.2014.01.120

[23] Aktar, S., Hossain, M.A., Shah, K., Mendez, A., de Figueiredo, C.C., Gasco, G., *et al.* (2024) Immobilization of Heavy Metals in Biochar Derived from Biosolids: Effect of Temperature and Carrier Gas. *Soil Systems*, **8**, Article 117. https://doi.org/10.3390/soilsystems8040117

[24] Batool, S., Idrees, M., Hussain, Q. and Kong, J. (2017) Adsorption of Copper (II) by Using Derived-Farmyard and Poultry Manure Biochars: Efficiency and Mechanism. *Chemical Physics Letters*, **689**, 190-198. https://doi.org/10.1016/j.cplett.2017.10.016

[25] Wang, Y. and Liu, R. (2018) H_2O_2 Treatment Enhanced the Heavy Metals Removal by Manure Biochar in Aqueous Solutions. *Science of The Total Environment*, **628**, 1139-1148. https://doi.org/10.1016/j.scitotenv.2018.02.137

[26] FAO (United Nations) (2019) Comprehensive Review and Situation Analysis for Rain Fed Cereal Production in the Kingdom of Saudi Arabia.

[27] Senoussi, A.H. and Kaddad, A. (2022) Impact of Emerging Camel Breeding Systems on Animal Welfare in the Algerian Northern Sahara—Case of a Breeding Farm in the Ouargla Region. Kasdi Merbah University Ouargla.

https://dspace.univ-ouargla.dz/jspui/handle/123456789/32704

[28] Wilson, K., Iqbal, J., Obaid Abdalla Obaid Hableel, A., Naji Khalaf Beyaha Alzaabi, Z. and Nazzal, Y. (2024) Camel Dung-Derived Biochar for the Removal of Copper(II) and Chromium(III) Ions from Aqueous Solutions: Adsorption and Kinetics Studies. *ACS Omega*, **9**, 11500-11509. https://doi.org/10.1021/acsomega.3c08230

[29] Jagadeesh, N. and Sundaram, B. (2023) Adsorption of Pollutants from Wastewater by Biochar: A Review. *Journal of Hazardous Materials Advances*, **9**, Article 100226. https://doi.org/10.1016/j.hazadv.2022.100226

[30] Rekos, K.C., Charisteidis, I.D., Tzamos, E., Palantzas, G., Zouboulis, A.I. and Triantafyllidis, K.S. (2022) Valorization of Hazardous Organic Solid Wastes Towards Fuels and Chemicals via Fast (Catalytic) Pyrolysis. *Sustainable Chemistry*, **3**, 91-111. https://doi.org/10.3390/suschem3010007

[31] Nandiyanto, A.B.D., Ragadhita, R. and Fiandini, M. (2022) Interpretation of Fourier Transform Infrared Spectra (FTIR): A Practical Approach in the Polymer/Plastic Thermal Decomposition. *Indonesian Journal of Science and Technology*, **8**, 113-126. https://doi.org/10.17509/ijost.v8i1.53297

[32] Igisu, M., Ueno, Y. and Takai, K. (2018) FTIR Microspectroscopy of Carbonaceous Matter in ~ 3.5 Ga Seafloor Hydrothermal Deposits in the North Pole Area, Western Australia. *Progress in Earth and Planetary Science*, **5**, Article No. 85. https://doi.org/10.1186/s40645-018-0242-1

[33] Faruruwa, M.D., Adamu, H.I., Adeyemi, M.M. and Tomori, W.B. (2024) Green Synthesis of Iron (III) Oxide (Fe_3O_4) Nanoparticles Using Citrus Sinensis Peel Extract for the Removal of Ciprofloxacin in Water. *Journal of Applied Sciences and Environmental Management*, **28**, 823-839. https://doi.org/10.4314/jasem.v28i3.23

[34] Taha, A.B., Essa, M.S. and Chiad, B.T. (2022) Spectroscopic Study of Iron Oxide Nanoparticles Synthesized via Hydrothermal Method. *Chemical Methodologies*, **6**, 977-984. https://doi.org/10.22034/CHEMM.2022.355199.1590

[35] Choudhury, A. and Lansing, S. (2020) Biochar Addition with Fe Impregnation to Reduce H2S Production from Anaerobic Digestion. *Bioresource Technology*, **306**, Article 123121. https://doi.org/10.1016/j.biortech.2020.123121

[36] Jabed, M.A. and Azmi Murad, M.A. (2024) Crop Yield Prediction in Agriculture: A Comprehensive Review of Machine Learning and Deep Learning Approaches, with Insights for Future Research and Sustainability. *Heliyon*, **10**, e40836. https://doi.org/10.1016/j.heliyon.2024.e40836

[37] Fito, J., Abewaa, M. and Nkambule, T. (2023) Magnetite-Impregnated Biochar of Parthenium Hysterophorus for Adsorption of Cr(VI) from Tannery Industrial Wastewater. *Applied Water Science*, **13**, Article No. 78. https://doi.org/10.1007/s13201-023-01880-y

[38] de Souza, T.F. and Dias Ferreira, G.M. (2024) Biochars as Adsorbents of Pesticides: Laboratory-Scale Performances and Real-World Contexts, Challenges, and Prospects. *ACS ES&T Water*, **4**, 4264-4282. https://doi.org/10.1021/acsestwater.4c00399

[39] Yang, J., Zhao, Y., Ma, S., Zhu, B., Zhang, J. and Zheng, C. (2016) Mercury Removal by Magnetic Biochar Derived from Simultaneous Activation and Magnetization of Sawdust. *Environmental Science & Technology*, **50**, 12040-12047. https://doi.org/10.1021/acs.est.6b03743

[40] Zheng, L., Gao, Y., Du, J., Zhang, W., Huang, Y., Wang, L., *et al.* (2020) A Novel, Recyclable Magnetic Biochar Modified by Chitosan-EDTA for the Effective Removal of Pb(II) from Aqueous Solution. *RSC Advances*, **10**, 40196-40205.

https://doi.org/10.1039/D0RA07499C

[41] Maity, D., Kale, S.N., Kaul-Ghanekar, R., Xue, J. and Ding, J. (2009) Studies of Magnetite Nanoparticles Synthesized by Thermal Decomposition of Iron (III) Acetylacetonate in Tri(Ethylene Glycol). *Journal of Magnetism and Magnetic Materials*, **321**, 3093-3098. https://doi.org/10.1016/j.jmmm.2009.05.020

[42] Hu, X., Ding, Z., Zimmerman, A.R., Wang, S. and Gao, B. (2015) Batch and Column Sorption of Arsenic onto Iron-Impregnated Biochar Synthesized through Hydrolysis. *Water Research*, **68**, 206-216. https://doi.org/10.1016/j.watres.2014.10.009

[43] Reguyal, F. and Sarmah, A.K. (2018) Site Energy Distribution Analysis and Influence of Fe3o4 Nanoparticles on Sulfamethoxazole Sorption in Aqueous Solution by Magnetic Pine Sawdust Biochar. *Environmental Pollution*, **233**, 510-519. https://doi.org/10.1016/j.envpol.2017.09.076

[44] Zhao, L., Zhao, Y., Nan, H., Yang, F., Qiu, H., Xu, X., *et al.* (2020) Suppressed Formation of Polycyclic Aromatic Hydrocarbons (PAHS) during Pyrolytic Production of Fe-Enriched Composite Biochar. *Journal of Hazardous Materials*, **382**, Article 121033. https://doi.org/10.1016/j.jhazmat.2019.121033

[45] Eltouny, N. and Ariya, P.A. (2014) Competing Reactions of Selected Atmospheric Gases on Fe_3O_4 Nanoparticles Surfaces. *Phys. Chem. Chem. Phys.*, **16**, 23056-23066. https://doi.org/10.1039/c4cp02379j

[46] Chen, X., Gao, X. and Wu, H. (2022) Characterization of Ashes from Co-Firing Biochar with Coal under Pulverized-Fuel Conditions. *ACS Engineering Au*, **2**, 397-405. https://doi.org/10.1021/acsengineeringau.2c00012

[47] Zhao, X., Hua, Q., Wang, C., Wang, X., Zhang, H., Zhang, K., *et al.* (2023) Study on Adsorption Performance and Mechanism of Peanut Hull-Derived Magnetic Biochar for Removal of Malachite Green from Water. *Materials Research Express*, **10**, Article 095504. https://doi.org/10.1088/2053-1591/acf756

[48] Yamashita, T. and Hayes, P. (2008) Analysis of XPS Spectra of Fe^{2+} and Fe^{3+} Ions in Oxide Materials. *Applied Surface Science*, **254**, 2441-2449. https://doi.org/10.1016/j.apsusc.2007.09.063

[49] Cruz-Lopes, L.P., Macena, M., Esteves, B. and Guiné, R.P.F. (2021) Ideal Ph for the Adsorption of Metal Ions Cr^{6+}, Ni^{2+}, Pb^{2+} in Aqueous Solution with Different Adsorbent Materials. *Open Agriculture*, **6**, 115-123. https://doi.org/10.1515/opag-2021-0225

[50] Foroutan, R., Peighambardoust, S.J., Mohammadi, R., Peighambardoust, S.H. and Ramavandi, B. (2022) Cadmium Ion Removal from Aqueous Media Using Banana Peel Biochar/Fe_3O_4/ZIF-67. *Environmental Research*, **211**, Article 113020. https://doi.org/10.1016/j.envres.2022.113020

[51] Lalhmunsiama, Gupta, P.L., Jung, H., Tiwari, D., Kong, S. and Lee, S. (2017) Insight into the Mechanism of Cd(II) and Pb(II) Removal by Sustainable Magnetic Biosorbent Precursor to Chlorella Vulgaris. *Journal of the Taiwan Institute of Chemical Engineers*, **71**, 206-213. https://doi.org/10.1016/j.jtice.2016.12.007

[52] Carnier, R., Coscione, A.R., Abreu, C.A.D., Melo, L.C.A. and Silva, A.F.D. (2022) Cadmium and Lead Adsorption and Desorption by Coffee Waste-Derived Biochars. *Bragantia*, **81**, e0622. https://doi.org/10.1590/1678-4499.20210142

[53] Mourdikoudis, S., Kostopoulou, A. and LaGrow, A.P. (2021) Magnetic Nanoparticle Composites: Synergistic Effects and Applications. *Advanced Science*, **8**, Article 2004951. https://doi.org/10.1002/advs.202004951

[54] Sarojini, G., Venkateshbabu, S. and Rajasimman, M. (2021) Facile Synthesis and

Characterization of Polypyrrole-Iron Oxide—Seaweed (PPY-Fe_3O_4-Sw) Nanocomposite and Its Exploration for Adsorptive Removal of Pb(II) from Heavy Metal Bearing Water. *Chemosphere*, **278**, Article 130400.
https://doi.org/10.1016/j.chemosphere.2021.130400

[55] Chen, K., He, J., Li, Y., Cai, X., Zhang, K., Liu, T., *et al.* (2017) Removal of Cadmium and Lead Ions from Water by Sulfonated Magnetic Nanoparticle Adsorbents. *Journal of Colloid and Interface Science*, **494**, 307-316.
https://doi.org/10.1016/j.jcis.2017.01.082

[56] Kaleem, M., Anjum Minhas, L., Zaffar Hashmi, M., Umer Farooqi, H.M., Waqar, R., Kamal, K., *et al.* (2024) Biogenic Synthesis of Iron Oxide Nanoparticles and Experimental Modeling Studies on the Removal of Heavy Metals from Wastewater. *Journal of Saudi Chemical Society*, **28**, Article 101777.
https://doi.org/10.1016/j.jscs.2023.101777